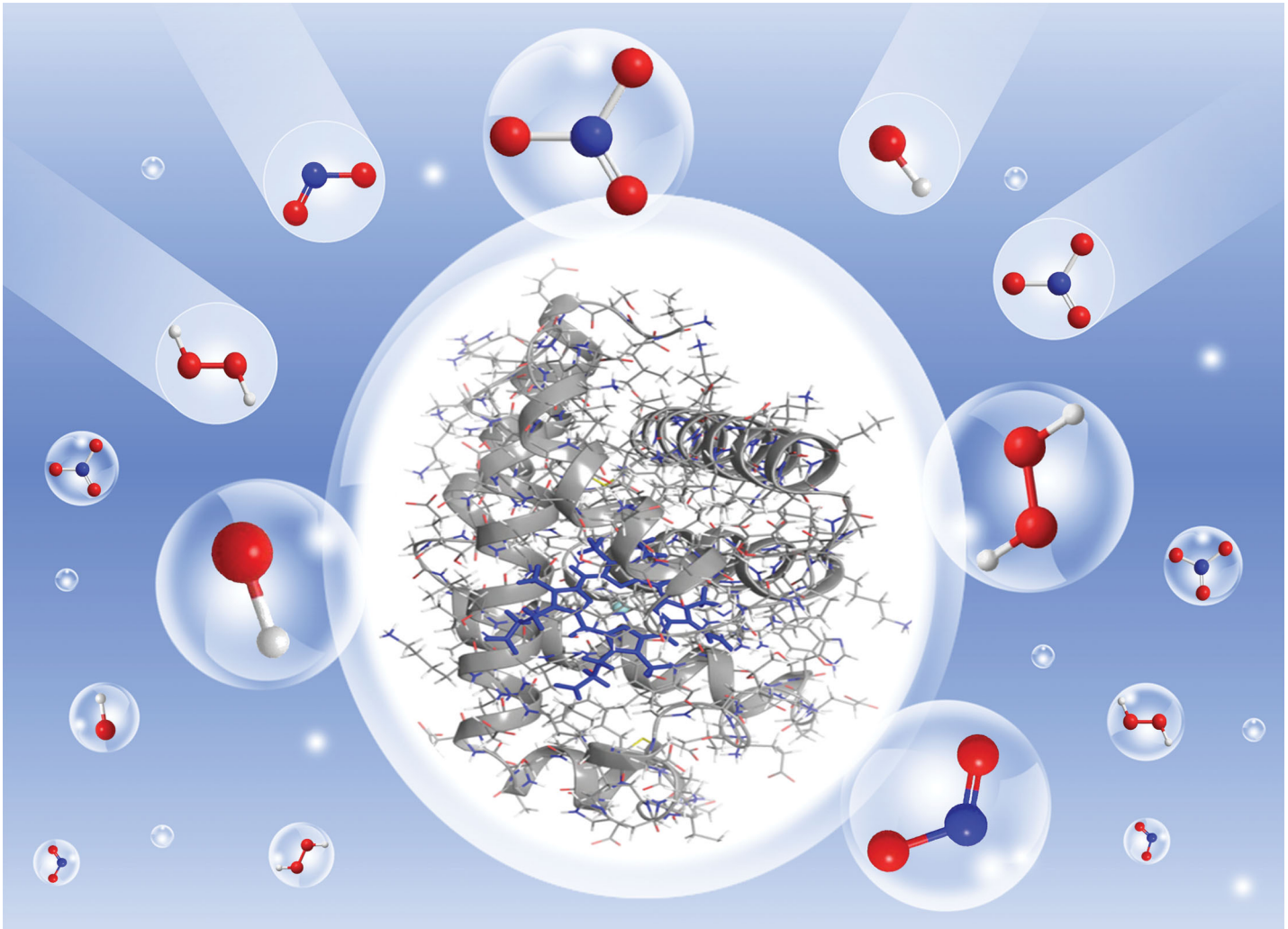

Highlighting research results from the Group of Prof. Masaharu Shiratani at the Faculty of Information Science and Electrical Engineering, Kyushu University, Fukuoka, Japan.

Impact of an ionic liquid on protein thermodynamics in the presence of cold atmospheric plasma and gamma rays

This paper reports the chemical and thermal denaturation of the protein myoglobin after cold atmospheric plasma and gamma treatments in the presence and absence of ionic liquids using various spectroscopic techniques. Additionally, molecular dynamics simulations were conducted to gain deeper insight into how the ionic liquids behave to protect the protein against the hydrogen peroxide generated by the plasma and gamma rays.

As featured in:

See Pankaj Attri, Art E. Cho, Kazunori Koga, Masaharu Shiratani *et al.*, *Phys. Chem. Chem. Phys.*, 2017, **19**, 25277.

ROYAL SOCIETY OF CHEMISTRY

rsc.li/pccp

Registered charity number: 207890

PCCP

PAPER

View Article Online
View Journal | View Issue

Cite this: *Phys. Chem. Chem. Phys.*, 2017, **19**, 25277

Impact of an ionic liquid on protein thermodynamics in the presence of cold atmospheric plasma and gamma rays†

Pankaj Attri,*[ab] Minsup Kim,[c] Eun Ha Choi,[a] Art E. Cho,*[c] Kazunori Koga*[b] and Masaharu Shiratani*[b]

Received 17th June 2017,
Accepted 19th July 2017

DOI: 10.1039/c7cp04083k

rsc.li/pccp

Cold atmospheric plasma and gamma rays are known to have anticancer properties, even though their specific mechanisms and roles as co-solvents during their action are still not clearly understood. Despite the use of gamma rays in cancer therapy, they have oncogenic potential, whereas this has not been observed for plasma treatment (to date). To gain a better understanding, we studied the action of dielectric barrier discharge (DBD) plasma and gamma rays on the myoglobin protein. We analyzed the secondary structure and thermodynamic properties of myoglobin after both treatments. In addition, in the last few years, ammonium ionic liquids (ILs) have revealed their important role in protein folding as co-solvents. In this work, we treated the protein with ammonium ILs such as triethylammonium methanesulfonate (TEMS) and tetrabutylammonium methanesulfonate (TBMS) and later treated this IL–protein solution with DBD plasma and gamma rays. In this study, we show the chemical and thermal denaturation of the protein after plasma and gamma treatments in the presence and absence of ILs using circular dichroism (CD) and UV-vis spectroscopy. Furthermore, we also show the influence of plasma and gamma rays on the secondary structure of myoglobin in the absence and presence of ILs or ILs + urea using CD. Finally, molecular dynamic simulations were conducted to gain deeper insight into how the ILs behave to protect the protein against the hydrogen peroxide generated by the DBD plasma and gamma rays.

Radiation is still the treatment that is most utilized for cancer patients in clinical management.[1–3] High and low linear energy transfer (LET) radiation is used to kill tumor cells at a minimum dose, to control the toxicity.[4] During cancer treatment, charged particles, X-rays and gamma rays are delivered to the body using a machine or through radioactive material located close to the cancer cells in the body. In addition, ionizing radiation is also used in pharmaceutical, agricultural, and other technological processes. Among all other forms of ionizing radiation, gamma rays are used more frequently due to their ease of accessibility and penetration power.[5] Furthermore, the structural and morphological changes in the biological system depend on the duration of the gamma ray exposure. In the last few decades, cold atmospheric plasma (CAP) has been studied to find a substitute for ionizing radiation in cancer treatment.

CAP has various medical applications,[6–8] including wound healing, sterilization, cancer treatment and blood coagulation.[9–12] CAP interacts with air to produce numerous radicals, including superoxide ($O_2^{\bullet-}$) and hydroxyl radicals ($^{\bullet}OH$), atomic oxygen (O), nitric oxide ($^{\bullet}NO$), *etc.* Throughout the plasma–liquid interactions, several moderately long lifetime reactive species are generated, including nitrites (NO_2^-), nitrates (NO_3^-), ozone (O_3) and hydrogen peroxide (H_2O_2).[13,14] CAP devices display significant anti-cancer capacity in both *in vitro*[15–19] and *in vivo* studies[20–23] for several cancer cell lines, including breast cancer,[24] skin cancer,[25] colorectal cancer,[26] cervical cancer,[27] lung cancer[28] and leukemia,[29] and studies have revealed their selective anti-cancer treatment modality, in contrast with conventional anti-cancer approaches. Selectivity was observed towards cell death in malignant cells by plasma,[16] whereas gamma rays don't seem to have a selective antitumor effect. But still, the protein folding studies using CAP are limited.[30–36]

Protein folding and its molecular mechanism play an important role in biological processes. During the period of evolution, certain

[a] *Plasma Bioscience Research Center/Department of Electrical and Biological Physics, Kwangwoon University, Seoul 01897, Korea. E-mail: chem.pankaj@gmail.com*
[b] *Faculty of Information Science and Electrical Engineering, Kyushu University, Fukuoka, Japan. E-mail: koga@ed.kyushu-u.ac.jp, siratani@ed.kyushu-u.ac.jp*
[c] *Department of Bioinformatics, Korea University, Sejong 02841, Korea. E-mail: artcho@korea.ac.kr*

† Electronic supplementary information (ESI) available. See DOI: 10.1039/c7cp04083k

protein sequences have molecular interactions that lead to their acquiring a particular structure, and these sequences are mutually supportive and cooperative, resulting in the function of the protein. The native structure of the protein has the lowest energy in the protein conformational space, and protein folding is affected by both intrinsic properties and extrinsic factors. The specific solvents are such extrinsic factors that change several aspects of the protein folding and stability.[37] Any change in the solvent conditions might also lead to changes in several key aspects of the protein stability and folding.[38–42] Ionic liquids (ILs) are composed of organic cations (generally large size) and counterions (generally compact size), and ILs are used to stabilize the protein structure,[38–43] refolding the protein,[44,45] and improving the catalytic activities.[46,47] Additionally, the thermodynamic properties of ILs with organic solvents have been studied for industrial processes.[48–51]

The unique properties and usage of ILs has provided a new revolution in materials science.[52] In recent years, the emphasis in many IL studies has now grown in the direction of medicine and life sciences. In a recent review, Egorova *et al.* suggested that bio-medical applications of ILs will be a major research trend in the near future.[53]

These properties of gamma rays, plasma and ILs are quite fascinating, but they have not been fully studied in combination. Recently, a few studies have been reported on the combination of ILs and gamma rays in various applications.[54,55] Kimura *et al.* produced cellulose gel using fluorescent carboxylate-based ionic liquids (ILs) in the presence of gamma-ray irradiation.[54] In another recent work, Morco *et al.* showed that the carbon steel corrosion rate seems to be slower and independent of gas in contact with an IL in the presence of gamma radiation.[55] As per the current status according to the literature, no such interaction studies of protein conformers with ILs and gamma rays have been conducted in the past. Similarly, only a few studies have reported the change in the protein conformation in the presence of ILs and plasma.[34,56] However, there are still no comparative studies on the protein conformation changes with ILs as a co-solvent in the presence of plasma and gamma rays. Therefore, in the present study, we used myoglobin as a model protein and triethylammonium methanesulfonate (TEMS) and tetrabutylammonium methanesulfonate (TBMS) as ammonium ILs to investigate the conformational changes in myoglobin after treatment with DBD plasma and gamma rays. We investigated the thermodynamic properties and structural changes in the myoglobin protein in the presence and absence of IL with DBD plasma and gamma rays in ambient air using CD spectroscopy and UV-vis spectroscopy. Furthermore, we also analyzed the generation of reactive oxygen and nitrogen species (RONS) in the phosphate buffer after irradiation with DBD plasma and gamma rays. Additionally, we also studied the molecular dynamic (MD) simulation of myoglobin + hydrogen peroxide (H_2O_2) with and without ILs (TEMS and TBMS). This study provides information on the role of ILs in protein folding during gamma ray and DBD plasma treatments.

Experimental section

Materials

The myoglobin protein, phosphate buffer (pH = 7.2), and TBMS were supplied by Aldrich Chemical Co. (USA). All chemicals and reagents were used without further purification. TEMS was prepared as per a previously reported work.[57] The concentrations of OH, NO, H_2O_2, NO_2^-, and NO_3^- were measured by the methods provided in our previous work.[12,13] NO is detected using 4-amino-5-methylamino-2′,7′-difluorofluorescein (DAF-FM); the excitation/emission maxima are 495/515 nm for DAF-FM-T (the product of the reaction between NO and DAF-FM). The detection of $^{\bullet}OH$ can be done using terephthalate anions obtained by mixing terephthalic acid (TA) in alkaline aqueous solution. These terephthalate anions react with $^{\bullet}OH$ to create highly fluorescent hydroxyterephthalate ions (HTA) and the excitation/emission maxima are 310/425 nm for the formation of HTA. The H_2O_2 concentration is measured using titanyl ions in the presence of sodium azide to control the H_2O_2 degradation by nitrites. The NO_2^- concentration is measured using Griess reagent supplied by Aldrich Chemical Co. (USA), whereas the NO_3^- concentration is obtained using an Acorn Series ION 6 meter (pH/mV/°C Meter), with a nitrate electrode, from Oakton Instruments, USA.

Dielectric barrier discharge

Experiments were carried out using a scalable DBD device, as described in previous research articles.[34,58] The device was set in ambient air at atmospheric pressure, and DBD plasmas were generated between the electrodes by supplying a 10 kHz AC high voltage (Logy Electric, LHV-09K). The discharge voltage and current were measured using a high-voltage probe (Tektronix, P6015A) and a Rogowski coil (URD, CTL-28-S90-05Z-1R1), respectively. The peak-to-peak discharge voltage and current were 9.2 kV and 0.2 A, and the corresponding discharge power density was 1.49 W cm^{-2}, which was deduced from a voltage/charge Lissajous plot.

Circular dichroism spectroscopy

CD spectroscopic studies were performed using a J-815 spectrophotometer (Jasco, Japan) equipped with a Peltier system to control the temperature.[30–34] The samples were pre-equilibrated at the desired temperature for 15 min, and the scan speed was fixed for adaptive sampling (error *F* 0.01) with a response time of 1 s with a 1 nm bandwidth. The secondary myoglobin structures were monitored using a 1.0 mm path length cuvette. The concentration for the secondary myoglobin structure was 0.2 mg ml^{-1}, with each spectrum being the average of six spectra. Each sample spectrum was obtained by subtracting the appropriate blank media without myoglobin from the experimental protein spectrum. The percentages of secondary structures were then calculated using Yang's method.[30]

Circular dichroism spectroscopy based urea studies

For each sample, the CD spectra were simultaneously measured from 200 to 250 nm at 25 °C. The ellipticity in the spectrum of

the native myoglobin in buffer (concentration of protein was 0.2 mg ml^{-1}) was assumed to correspond to 100% folded protein, and the ellipticity in the spectrum of myoglobin with 9.0 M urea was assumed to correspond to unfolded protein. The CD spectra displayed for myoglobin have two well-pronounced minima at ≈210 and ≈222 nm resembling those typical for polypeptide chains that are mostly organized in an α-helix conformation, so we studied the change in ellipticity at 222 nm to understand the change in α-helix conformation as the function of the urea concentration.

Temperature stability studies

For each sample, the CD spectra were simultaneously measured at 222 nm as a function of temperature from 25 to 100 °C. The sample was placed in a sealed cuvette to prevent water evaporation, and the 222 nm ellipticity in the spectrum of native myoglobin in buffer (concentration of protein was 0.2 mg ml^{-1}) at 25 °C was assumed to correspond to 100% folded protein, and at 100 °C it was assumed to be unfolded protein, and the folded fraction was computed as:

$$\text{Fraction folded} = \frac{A_{222} - A_u}{A_f - A_u}$$

In this method, A_{222} is the absorbance between 30 and 100 °C, A_u is the absorbance of the unfolded protein at 100 °C, and A_f is the absorbance of the folded protein at 30 °C. We have studied the change in ellipticity at 222 nm to understand the change in α-helix conformation as a function of the temperature.

UV-visible spectroscopy

A 0.5 mg ml^{-1} concentration of the protein sample was used for UV-vis spectroscopy. The heme moiety in myoglobin exhibits a strong absorbance band at 409 nm and also displays a strong positive signal.[59] The 409 nm absorbance can be used to quantify the fraction of the folded protein, and the fraction of the folded protein was computed from the 409 nm absorbance following previous reports.[60] Briefly, the 409 nm absorbance in the spectrum of native myoglobin in buffer was assumed to correspond to 100% folded protein, and the 409 nm absorbance in the spectrum of myoglobin with 9.0 M urea was assumed to correspond to 0% folded protein. The folded fraction was computed as:

$$\text{Fraction folded} = \frac{A_{409} - A_u}{A_f - A_u}$$

In this method, A_{409} is the absorbance, A_u is the 409 nm absorbance of the unfolded protein, and A_f is the absorbance of the folded protein.

pH and temperature measurement

After the plasma was exposed for 6, 12, and 24 min in buffer, the pH and temperature of the solution were measured using Horiba scientific instruments. All measurements were carried out in triplicate.

Molecular dynamics simulation

The crystal structures of myoglobin were obtained from the (RCSB) protein data bank website (http://www.rcsb.org; the PDB IDs were 1MBN).[30] These structures were treated with the Protein Preparation Wizard of the Schrödinger suite for molecular dynamics (MD) simulations. All water and heat molecules were eliminated, and hydrogen's were added and minimized using IMPACT 6.6,[61] and MD simulations were performed using Desmond 4.4.[62] The simulation systems were prepared with the Desmond system builder, and the box shape of the systems was orthorhombic, with the size determined using the 10 Å buffer distance between the solute structures and the simulation box boundary. The systems were solvated with TIP3P model water. Na^+ or Cl^- ions were added to the systems to neutralize the total charges of the system. Hydrogen peroxide (H_2O_2) molecules were added to achieve 20% concentration of the systems. The charges of H_2O_2 were determined from the electrostatic potential (ESP) charge fitting with Jaguar version 8.7[63] (Schrödinger, LLC, New York, NY, 2015), using the basis set and function of B3LYP/6-31G**. The MD simulations were performed in the (*NPT*) ensemble with the OPLS2005 all atom force field. A reference temperature of 300 K and pressure of 1 atm were maintained by the Nose–Hoover thermostat and the Martyna–Tobias–Klein barostat. Before performing the main simulations, a series of minimizations and short MD simulations were performed to relax the model system.

Sample preparation

The protein was added to 2 ml screw-capped vials in phosphate buffer, at 25 °C and kept for 4 h to attain complete equilibrium after blending the solution. Similarly, 400 mM of ILs (TEMS or TBMS) was dissolved in the mixture of protein and phosphate buffer at 25 °C, and the solution was kept for 4 h to attain complete equilibrium after blending the solution. The samples were treated at 6 mm distances from the plasma for 5, 10, and 20 min, at the humidity of 45%, and were then incubated for 4 h at room temperature after plasma treatment. Three samples were treated for each condition to minimize the error.

Statistical analysis

All of the values are represented by the mean ± S.D. of the indicated number of replicates.

Results and discussion

Thermal or chemical induced unfolding studies offer a significant understanding of the thermodynamics of protein folding.[38,60,64] Therefore, in this work we study the thermal and chemical denaturation of the myoglobin protein after DBD plasma and gamma ray treatment. Previous studies show that triethylammonium methanesulfonate (TEMS) IL provides a suitable medium for lignin to confirm electrolysis at higher potentials.[65] In another study, a TEMS IL dopant extended the thermal stability of a Nafion 117 membrane.[57] Therefore, in our study, we used the TEMS (400 mM) and TBMS (400 mM) ILs to

investigate the effect of the cation on the stability of the protein in the presence of plasma and gamma ray treatments.

Analysis of reactive species generation, pH and temperature change in buffer solution after the plasma and gamma ray treatments

DBD plasma and gamma ray irradiation on phosphate buffer generates reactive oxygen and nitrogen species (RONS), as displayed in Fig. 1 and 2. After the treatments, we analysed the formation of RONS, such as $^{\bullet}OH$, H_2O_2, $NO^{\bullet}$, NO_2^-, and NO_3^-. Fig. 1 shows that after DBD plasma treatment for 6, 12, and 24 min, we analysed the relative mean fluoresce values of the $^{\bullet}OH$ and $NO^{\bullet}$ radicals. This figure reveals that as the treatment time increases, the relative mean fluorescence values also increase for both radicals. Therefore, the intensity of both radicals is directly related to the treatment time, meaning that an increase in treatment time increases the production of $^{\bullet}OH$ and $NO^{\bullet}$ radicals in the buffer. Additionally, the concentration of H_2O_2, NO_2^-, and NO_3^- was also determined after the DBD plasma treatment for the above mentioned time intervals. The concentration of H_2O_2 was $\approx$18, 50, and 75 μM after the DBD plasma treatment for 6, 12, and 24 min. One of the main sources of H_2O_2 formation was the plasma interaction with humidity (H_2O) in the air and water molecules on the surface of the buffer. This generates $^{\bullet}OH$ radicals and further reaction results in the formation of H_2O_2. On the other hand the NO_2^- concentration for 6, 12, and 24 min of plasma treatment was $\approx$110, 162, and 316 μM, respectively. Similarly, the concentration of NO_3^- was $\approx$135, 215, and 458 μM for 6, 12, and 24 min of the DBD plasma treatment, respectively, although the generation of NO_2^- and NO_3^- ions is a result of the reaction between the plasma and air. Some of the reactions that result in the formation of $^{\bullet}OH$, H_2O_2, $NO^{\bullet}$, NO_2^-, and NO_3^- are given below.

$$e + O_2 \rightarrow e + 2O \quad (1)$$

$$O + O_2 \rightarrow O_3 \quad (2)$$

$$e + N_2 \rightarrow e + 2N \quad (3)$$

$$O + N \rightarrow NO^{\bullet} \quad (4)$$

$$4NO^{\bullet} + O_2 + 2H_2O \rightarrow 4NO_2^- + 4H^+ \quad (5)$$

$$e + H_2O \rightarrow {}^{\bullet}OH + H^{\bullet} \quad (6)$$

$${}^{\bullet}OH + {}^{\bullet}OH \rightarrow H_2O_2 \quad (7)$$

$$H_2O_2 + {}^{\bullet}OH \rightarrow H_2O + HO_2^{\bullet} \quad (8)$$

$$H_2O + HO_2^{\bullet} \rightarrow H^+ + O_2^{\bullet -} \quad (9)$$

$$2O_2^{\bullet -} + 2H^+ \rightarrow H_2O_2 + O_2 \quad (10)$$

$$O_2^{\bullet -} + NO^{\bullet} \rightarrow ONOO^- \quad (11)$$

$$ONOO^- + H_2O_2 \rightarrow {}^1O_2 + H_2O + NO_2^- \quad (12)$$

$$H^+ + ONOO^- \rightarrow ONOOH \quad (13)$$

$$ONOOH \rightarrow {}^{\bullet}NO_2 + {}^{\bullet}OH \quad (14)$$

$$2NO_2 + H_2O \rightarrow 2H^+ + NO_3^- + NO_2^- \quad (15)$$

$$NO^{\bullet} + HO_2^{\bullet} \rightarrow O_2 + HNO \quad (16)$$

$$NO_3^- + NO \rightarrow NO_2^- + {}^{\bullet}NO_2 \quad (17)$$

Nevertheless, we analysed $^{\bullet}OH$, H_2O_2, $NO^{\bullet}$, NO_2^-, and NO_3^- after the gamma treatment at different absorbed doses. Fig. 2 shows that as the gamma radiation absorbed dose increased from 220 to 1130 Gy, the relative mean fluorescence values also

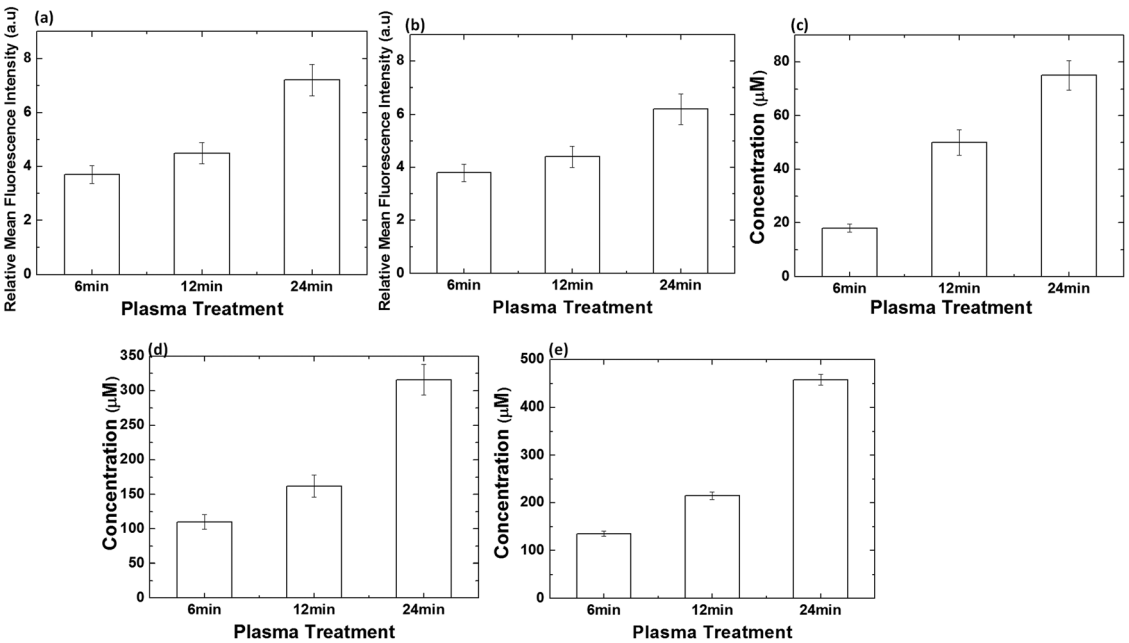

Fig. 1 Analysis of reactive oxygen and nitrogen species such as (a) $^{\bullet}OH$; (b) $NO^{\bullet}$; (c) H_2O_2; (d) NO_2^- and (e) NO_3^- detection in phosphate buffer after treatment with DBD plasma for different time intervals such as 6, 12 and 24 min.

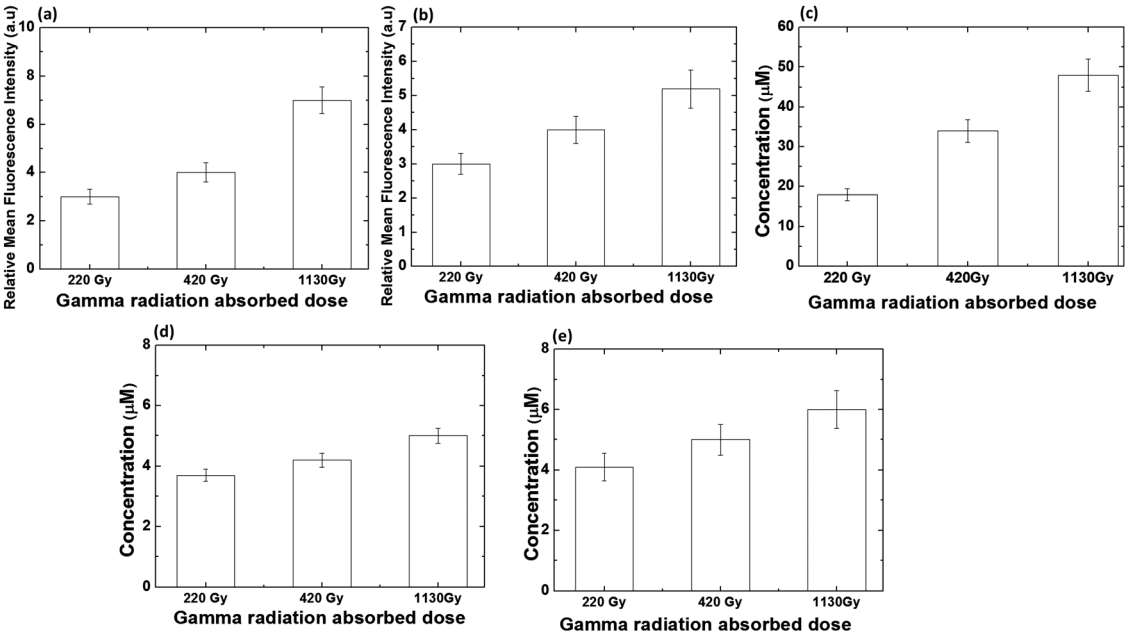

Fig. 2 Analysis of reactive oxygen and nitrogen species such as (a) $^{\bullet}OH$; (b) $NO^{\bullet}$; (c) H_2O_2; (d) NO_2^- and (e) NO_3^- detection in phosphate buffer after treatment with different gamma ray absorbed doses such as 220, 420 and 1130 Gy.

increased for both radicals ($NO^{\bullet}$ and $^{\bullet}OH$). This means that the concentration of radicals in the buffer solution increases as the absorbed dose of the gamma rays increases. Furthermore, the concentration of H_2O_2, NO_2^-, and NO_3^- was also investigated after variations in the gamma irradiation. The H_2O_2 concentration was $\approx$17, 34, and 48 μM for the 220, 420 and 1130 Gy absorbed dose, respectively. Although the concentration of NO_2^- was $\approx$3.7, 4.2, and 5 μM and the concentration of NO_3^- was $\approx$4.1, 5, and 6 μM for a 220, 420 and 1130 Gy absorbed dose, respectively. This increase in the concentration of H_2O_2, NO_2^-, and NO_3^- also follows similar behavior as $^{\bullet}OH$ and $NO^{\bullet}$ radicals since the absorbed dose increases the concentration of radicals and the number of ions increases. Nevertheless, after different treatments with gamma radiation, the concentrations of H_2O_2 were higher than the concentrations of NO_2^- and NO_3^- because the main source of H_2O_2 was the $^{\bullet}OH$ (eqn (7)), and it is well known that water radiolysis by gamma rays results in the generation of $^{\bullet}OH$.[66] Therefore, the formation of H_2O_2 was greater during gamma irradiation.

Similar to the DBD plasma treatment, the concentration of H_2O_2, NO_2^-, and NO_3^- increases as the absorbed dose of gamma rays increases. On comparing the production of H_2O_2 in buffer upon DBD plasma treatment and gamma ray irradiation, we observe that in DBD plasma, slightly more H_2O_2 is produced compared to gamma ray treatment. While NO_2^- and NO_3^- ions are generated more in DBD plasma than with gamma rays, this might be due to differences in the environmental conditions of both treatments. We were not able to measure the environmental conditions during the gamma ray treatment due to the radiation problem, whereas for DBD plasma treatment, we used the atmospheric conditions with humidity of 45%. The difference in the environmental conditions during both treatments can be one of the reasons for the high RNS species that formed in the DBD plasma treatment. Nonetheless, the concentrations of H_2O_2 produced by the 24 min plasma and 1130 Gy gamma ray treatments were not much different from each other (75 μM after plasma and 48 μM after gamma rays) because the main reaction to generate H_2O_2 was very similar for the plasma and gamma rays, as described above. In addition, there was no change in the pH and temperature after both treatments (plasma and gamma rays (data not shown)).

Chemical denaturation of myoglobin before and after treatment with plasma and gamma rays

We studied the absorption measurements for the protein in the presence of TEMS or TBMS ILs in phosphate buffer solution. To illustrate the chemical unfolding of the myoglobin protein, we studied the absorbance intensity at 409 nm as a function of the urea concentration. The changes in the absorbance at 409 nm correlate with the unfolding of the myoglobin, and the absorbance at 409 nm for the native myoglobin protein in buffer is assumed to correspond to 100% folded protein (A_f) at a 0 M urea concentration, and the absorbance at 409 nm with 9.0 M urea is assumed to be the unfolded myoglobin protein (A_u).

$$\text{Fraction folded} = \frac{A_{409} - A_u}{A_f - A_u}$$

A_{409} is the absorbance in the presence of urea (except 0 and 9 M). Fig. S1 (ESI†) shows that the 50% fraction of the proteins was denatured at 6.3 ± 0.2 M urea. While after DBD plasma treatment for 6, 12, and 24 min in ambient air, a 50% fraction of the protein was denatured at 5.9 ± 0.2, 5.4 ± 0.3 and

4.1 ± 0.2 M of urea, although 50% of the protein solution in the presence of TEMS and TBMS was denatured by urea at 6.3 ± 0.1 and 6.1 ± 0.2 M urea, respectively. Hence, the chemical denaturation of the protein in the presence of TEMS was similar to the control protein, but the denaturation of the protein in the presence of TBMS starts at a slightly lower concentration of urea. On the other hand the 50% fraction of the chemical denaturation of the protein + TEMS after treatment with plasma for 6, 12, and 24 min occurred at 5.7 ± 0.2, 5.3 ± 0.1 and 5 ± 0.2 M urea, and the 50% fraction of the chemical denaturation of the protein + TBMS after treatment with the plasma for 6, 12, and 24 min occurred at 5.8 ± 0.4, 5.5 ± 0.2 and 5.2 ± 0.3 M urea. This reveals that although TBMS can't stabilize the protein further compared to TEMS for chemical denaturation, both ILs have almost similar counteraction properties against the urea induced denaturation in the presence of plasma. Specifically, after 24 min of plasma treatment both ILs revealed a significant contribution to protection of the protein structure against urea-plasma induced denaturation.

A 50% fraction of myoglobin was denatured at 5.8 ± 0.2, 5.3 ± 0.1, and 4.6 ± 0.26 M urea concentration after treatment with gamma rays for the absorbed dose of 220, 420, and 1130 Gy, respectively (Fig. S2, ESI†). These outcomes illustrate that as the absorbed dose of gamma rays increases, the denaturation of myoglobin occurs at a lower urea concentration. The minimum and maximum chemical denaturation arise at 220 Gy and 1130 Gy, respectively. Later, we treated the protein at different absorbed doses of gamma rays in the presence of both ILs, such as TEMS and TBMS. Fig. S2 (ESI†) shows that the protein denatured at 6.1 ± 0.1, 5.7 ± 0.3, and 5.2 ± 0.2 M urea in the presence of TEMS, and 6.1 ± 0.1, 6 ± 0.2, and 5.1 ± 0.3 M urea in the presence of TBMS, for the absorbed doses of 220, 420, and 1130 Gy, respectively. Hence, both ILs can protect the protein against urea-gamma induced denaturation.

Secondary structural changes of the protein after DBD and gamma treatment in the presence and absence of urea

The structural modification of myoglobin after DBD plasma and gamma ray treatments were studied using circular dichroism (CD) spectroscopy. The far-UV CD spectrum of myoglobin shows the secondary structural change of the protein after different treatments. The myoglobin has two minima at ≈210 and ≈222 nm that resemble the polypeptide chain. For the control protein (without treatment), the α-helical content of myoglobin was 63%, but it changed to 60%, 59% and 57% after treatment with plasma for 6, 12, and 24 min, respectively, as shown in Fig. 3. After the addition of ILs, TEMS, and TBMS, the

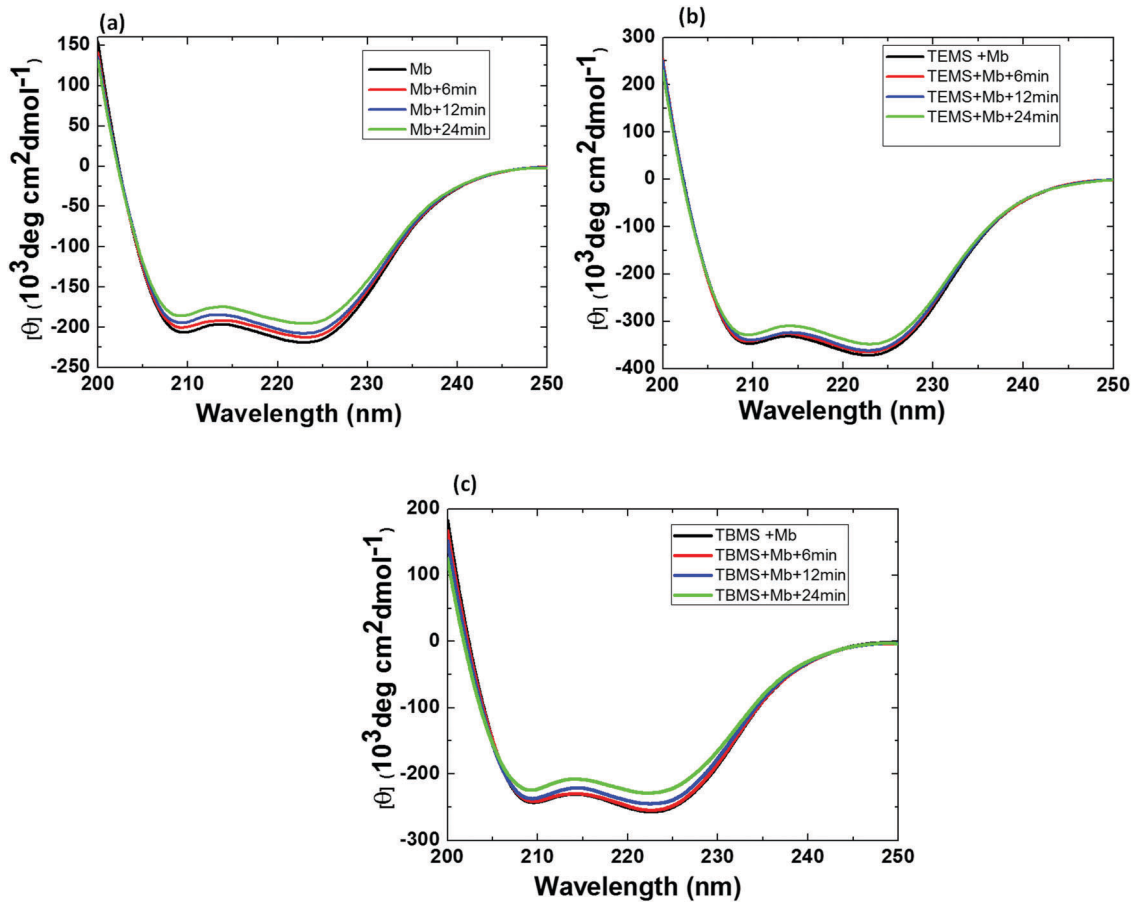

Fig. 3 Analysis of myoglobin secondary structure change using CD spectroscopy after treatment with DBD plasma for different time intervals such as 6, 12 and 24 min: (a) control myoglobin, (b) myoglobin + TEMS and (c) myoglobin + TBMS.

α-helical content changes to 62% and 60%, respectively. This shows that after the incubation of the protein with TEMS and TBMS IL, there is a slight decrease in the α-helical content of myoglobin while the α-helical content changed to 62.7%, 62.8% and 60% for myoglobin + TEMS in the presence of plasma treatment for 6, 12, and 24 min, respectively. After the plasma treatment of the solution of myoglobin + TBMS for 6, 12, and 24 min the α-helical content changes to 60%, 56% and 52%, respectively (Fig. 3). These data illustrate that TEMS can control the secondary structure of the protein more compared to TBMS in the presence of plasma treatment.

Fig. 4 reveals that the α-helical content of myoglobin was 58%, 57%, and 54%, after the gamma ray treatment for an absorbed dose of 220, 420 and 1130 Gy, respectively. Subsequently, upon the addition of TEMS to the myoglobin solution, the percentage of α-helices changes to 58%, 58%, and 57%, when irradiated with gamma rays at an absorbed dose of 220, 420 and 1130 Gy, respectively. Moreover, the α-helical content in myoglobin + TBMS changed to 58%, 58%, and 57%, after the treatment of gamma rays at the absorbed dose of 220, 420 and 1130 Gy (Fig. 4). This data shows that both ILs protect the secondary structure of the protein in a similar way after the gamma ray treatment.

The α-helical structure of protein was investigated at various concentrations of urea, in the presence and absence of plasma and gamma ray treatments. The observed peak at ≈222 nm resembles that of the polypeptide chain that is mainly for the secondary structure of the protein. We observed that as the urea concentration increases, the ellipticity value of the protein at ≈222 nm decreases. The ellipticity value of control myoglobin increases slightly up to 5 M urea, and later, the slope is quite steep between 6 to 8 M urea and further becomes constant at 9 M urea (Fig. S3, ESI†). After the plasma treatment for 6, 12, and 24 min, the slope follows a similar path, and the ellipticity for 24 min plasma treatment was highest and was the least for the 6 min plasma treatment, as shown in the Fig. S3 (ESI†). In the presence of the plasma-treated samples, the ellipticity at 222 nm is higher than the respective corresponding control values for all studied samples, and at all treated conditions, except for 8 and 9 M urea for the myoglobin + TEMS and + TBMS systems. The difference in the ellipticity among the different plasma treatment conditions is the highest for the TBMS + myoglobin as compared to TEMS + myoglobin.

For the gamma treatment at absorbed doses of 220, 420 and 1130 Gy, the ellipticity values were higher than those of the control sample (myoglobin protein) over a concentration range from 0 to 8 M, and these meet each other at 9 M urea, as illustrated in Fig. S4 (ESI†). At 9 M urea, the structure of myoglobin is completely denatured, so no change in the ellipticity is observed. For myoglobin + TEMS and + TBMS, the ellipticity values increase slightly up to 5 M urea; but the slope is quite steep between

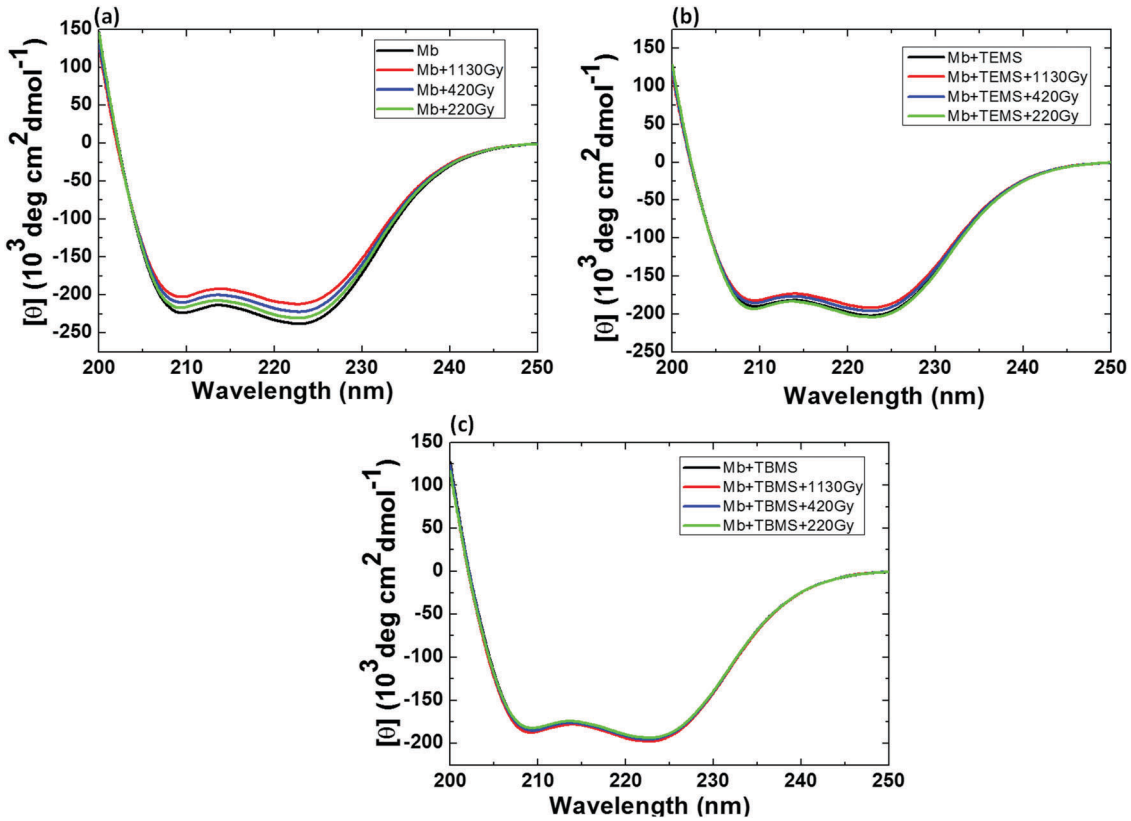

Fig. 4 Analysis of myoglobin secondary structure change using CD spectroscopy after treatment with different gamma ray absorbed doses such as 220, 420 and 1130 Gy: (a) control myoglobin, (b) myoglobin + TEMS and (c) myoglobin + TBMS.

5 and 7 M urea and then becomes constant at above 8 M urea. In both cases (myoglobin + TEMS and + TBMS), there is less of a difference in the ellipticity values after the gamma treatment, as compared to the control gamma treated samples (without ILs).

Thermal denaturation of the protein with or without ILs in the presence and absence of DBD plasma and gamma ray treatment

We used CD spectroscopy to understand the thermal denaturation of the myoglobin protein system in all studied systems, as shown in Fig. 5, 6, and Table S1 (ESI†). The melting temperature (T_m), is an important thermodynamic parameter that is used to understand the thermal unfolding of the protein. The T_m value of the myoglobin control (without treatment) in phosphate buffer was 83 °C while the T_m value changed to 81, 75, and 74 °C, after the treatment with DBD plasma for 6, 12, and 24 min, as shown in Fig. 5. The T_m values in myoglobin + TEMS and + TBMS were 83.4 and 76 °C, and this shows that the TBMS solution changes the thermodynamic properties of the protein. However, the TEMS solution slightly improves the thermodynamic properties, and these results are well correlated with chemical denaturation studies where the TBMS + myoglobin solution denatures at a low urea concentration as compared to the TEMS + myoglobin solution. Nevertheless, after the plasma treatment for 6, 12, and 24 min in the presence of TEMS as a co-solvent, the T_m values change to 82.5, 81.7 and 81.1 °C, respectively (Fig. 5 and Table S1, ESI†). For TBMS as a co-solvent, the T_m values change to 76, 75.6 and 73.1 °C. This shows that after the plasma treatment, both ILs control the protein structure thermodynamics very well compared to that without the IL plasma treatment. However, TEMS as a co-solvent protects the myoglobin structure in a better way compared to TBMS.

In another study, myoglobin was treated with gamma rays at an absorbed dose of 220, 420 and 1130 Gy, and the T_m of the protein was 82, 81, and 80 °C whereas it seemed to be 83 °C for the control protein (without gamma treatment) (Fig. 6 and Table S1, ESI†). When we added TEMS as a co-solvent to the myoglobin protein solution, and this solution was later irradiated with gamma rays, the T_m values were 82.3, 81.1, and 80 °C, for a 220, 420 and 1130 Gy absorbed dose, respectively. On the other hand, with the presence of TBMS as a co-solvent, the T_m values were 74.6, 74.3, and 70.9 °C, for a 220, 420 and 1130 Gy absorbed dose of gamma rays, respectively (Fig. 6 and Table S1, ESI†). This indicates that TEMS + myoglobin can counter gamma rays in better ways as compared to TBMS + myoglobin. Also, the T_m values of the protein or protein + ILs decrease for gamma rays

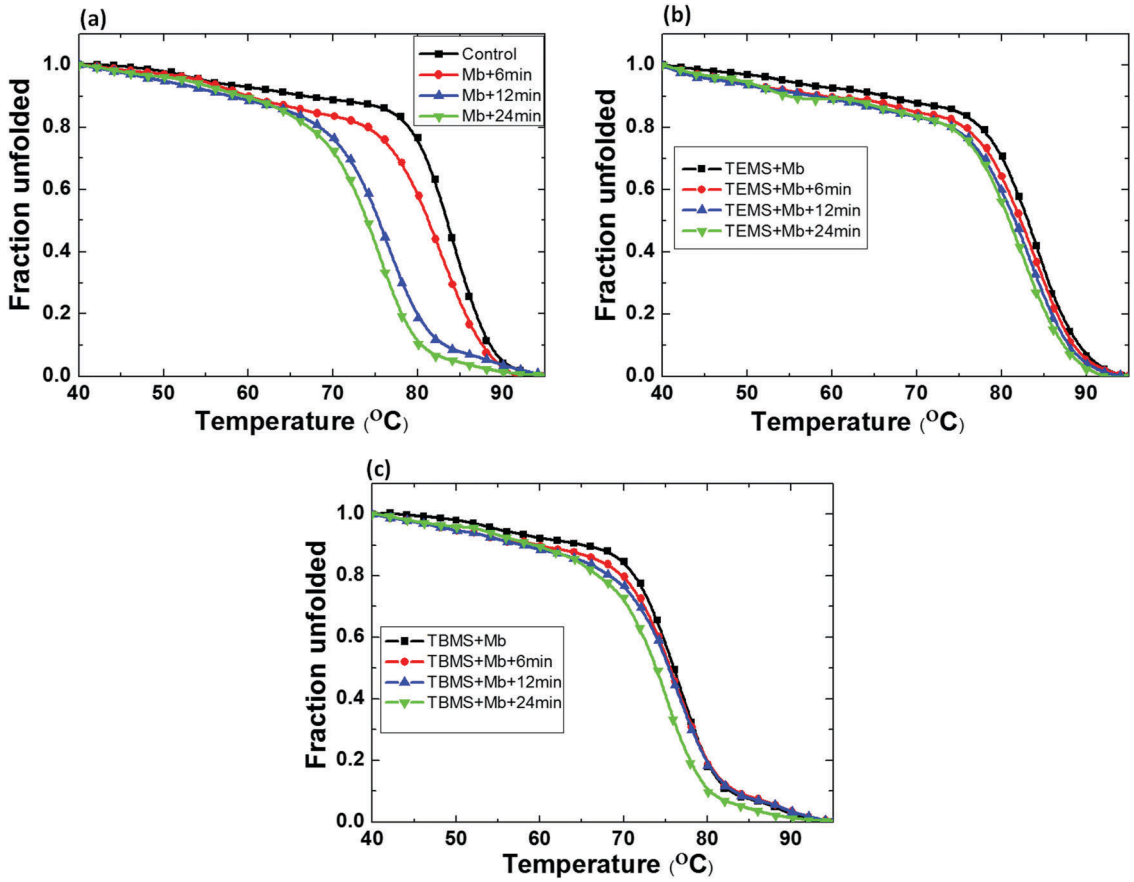

Fig. 5 Thermal denaturation profile of myoglobin protein after treatment with DBD plasma for different time intervals such as 6, 12 and 24 min: (a) control myoglobin, (b) myoglobin + TEMS and (c) myoglobin + TBMS.

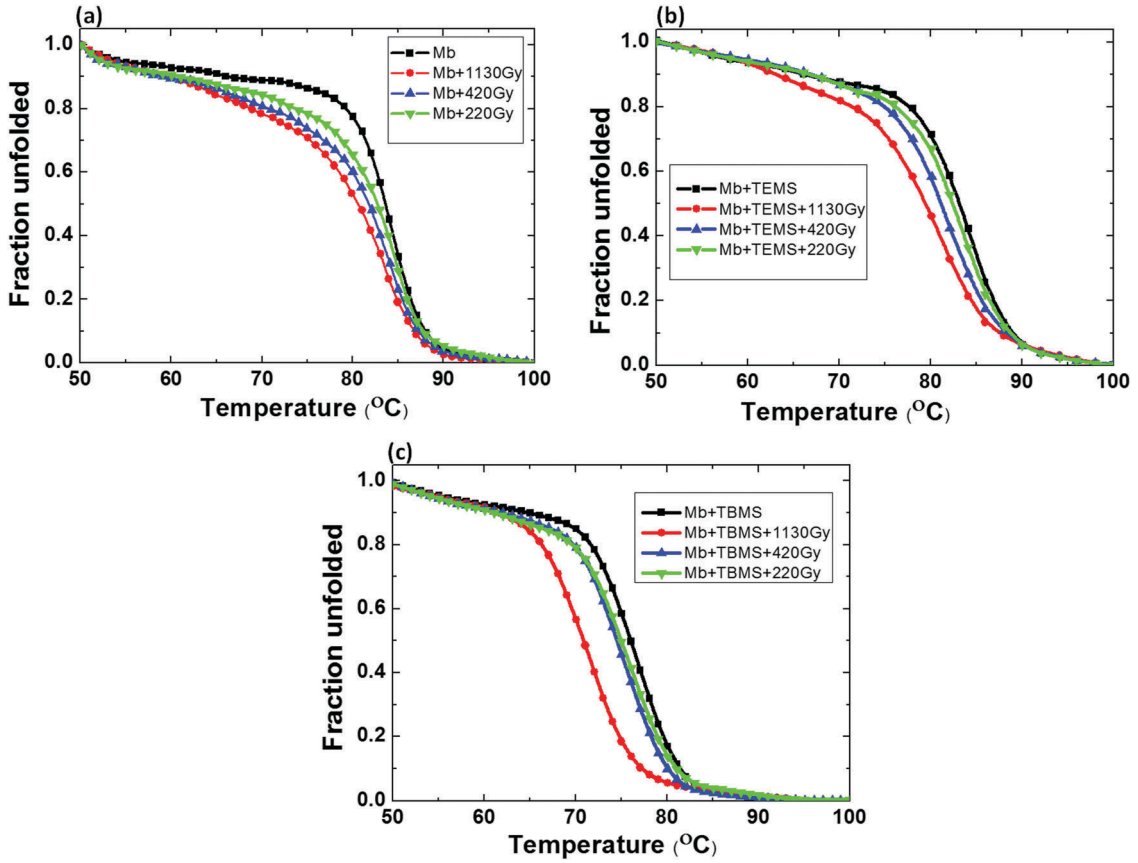

Fig. 6 Thermal denaturation profile of myoglobin protein after treatment with different gamma ray absorbed doses such as 220, 420 and 1130 Gy: (a) control myoglobin, (b) myoglobin + TEMS and (c) myoglobin + TBMS.

compared to plasma. Furthermore, we have studied MD simulations to understand the action of hydrogen peroxide that was produced in approximately the same concentration after the plasma and gamma treatment in buffer.

Molecular dynamics simulation of myoglobin in the presence of H_2O_2 with or without ILs

The presence of ILs in the myoglobin protein influences the denaturation action of hydrogen peroxide on the myoglobin protein structure. We studied MD simulations to analyze this. Three types of MD simulation systems were studied:

(1) myoglobin protein solvated in phosphate buffer (20 mM),

(2) myoglobin protein + buffer + 20% hydrogen peroxide, and

(3) myoglobin protein + buffer + 20% hydrogen peroxide + ILs (TEMS or TBMS).

We used the root-mean-square atomic positional deviation (RMSD) values to study the structural stabilities of myoglobin for various environmental conditions. The hydrogen peroxide molecules were uniformly distributed in buffer solutions but seemed to condense within 1 Å of the surface of the myoglobin protein over a very short duration. Fig. 7 reveals the RMSD values under all treatment conditions. However, in the presence of 20% hydrogen peroxide solution, the structure of myoglobin experienced conformational changes. These changes showed higher RMSD values for the myoglobin protein in the presence of hydrogen peroxide, after simulation for 50 ns when compared to in the absence of hydrogen peroxide solution. The RMSD value for the myoglobin protein in buffer was 1.75, but after treatment with hydrogen peroxide solution, the RMSD value increased to 2.17 with a change in the standard deviation value of 0.29, as seen in Table S2 (ESI†). This indicates that the presence of the hydrogen peroxide solution destabilizes the myoglobin structure. Furthermore, we considered the MD simulation to analyse the action of the TEMS and TBMS ILs on the myoglobin protein. Fig. 7 shows that myoglobin in the presence of 20% TEMS or 20% TBMS with buffer solution maintained a stable conformation for 50 ns. Moreover, we also measured the RMSD for myoglobin + buffer + hydrogen peroxide + ILs. The RMSD value for the myoglobin protein + buffer + TEMS or + TBMS was 2.54 and 2.97, with a standard deviation of 0.34 and 0.39, respectively. Nevertheless, after treatment with hydrogen peroxide, the RMSD for myoglobin + buffer + TEMS increased to 2.68, with a change in the standard deviation of 0.30 (Table S2, ESI†). However, the RMSD for myoglobin + buffer + TBMS + hydrogen peroxide was 3.10, with a standard deviation of 0.44, as seen in Table S2 (ESI†). Therefore, we conclude that in the presence of TEMS, the protein structure is

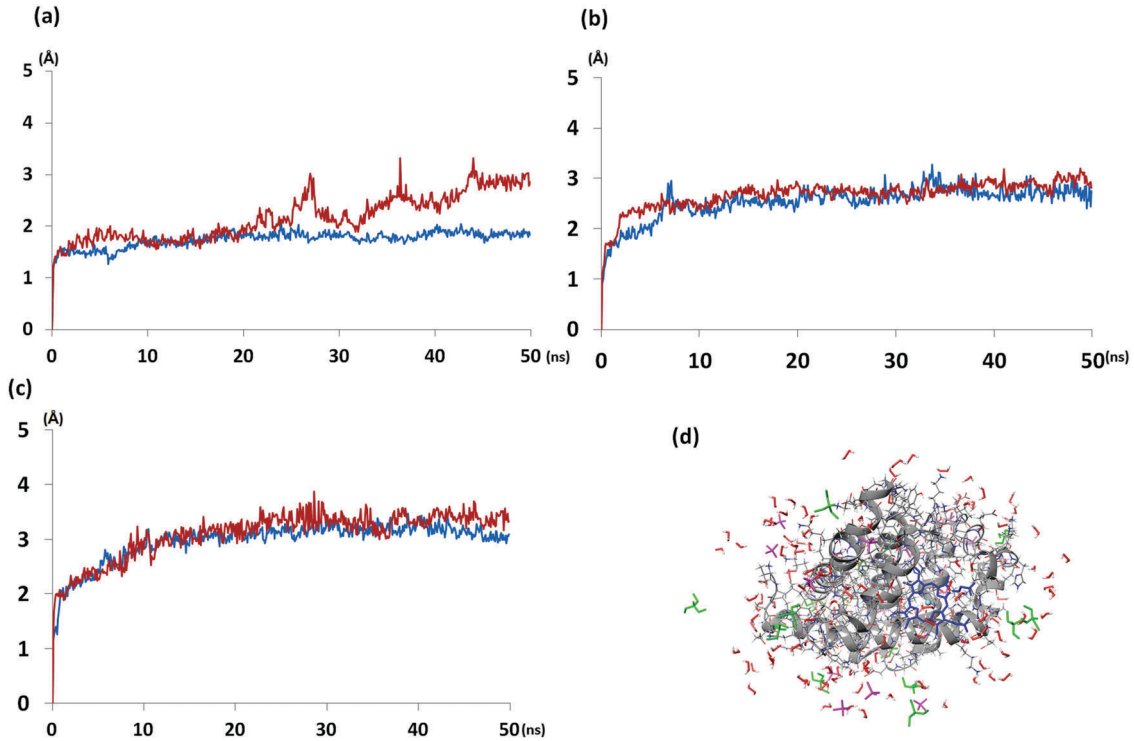

Fig. 7 MD simulation of myoglobin, (a) RMSD plots of myoglobin in phosphate buffer and 20% H_2O_2; (b) RMSD plots of myoglobin in phosphate buffer, 20% H_2O_2 + 20% TEMS; (c) RMSD plots of myoglobin in phosphate buffer, 20% H_2O_2 + 20% TBMS; (d) snapshot of myoglobin + 20% H_2O_2 + 20% TEMS (gray ribbon and wire – myoglobin, blue – heme group, green – TEMS and red – H_2O_2).

more stabilized as compared to in TBMS, and these results correlate well with our experimental data above.

Conclusion

In the present work, we checked the change in the secondary structure, chemical denaturation and thermal denaturation of myoglobin protein with and without ILs after DBD plasma and gamma ray treatment. During the RONS analysis in buffer, we observed a slight difference in the H_2O_2 concentrations generated in buffer after plasma and gamma ray treatment, but the concentrations of NO_2^- and NO_3^- were quite a bit higher for the plasma treated buffer than for the gamma treatment. The chemical denaturation of the protein is synchronized with the plasma or gamma ray treatment. After treatment with plasma or gamma rays, the protein denatures at a lower urea concentration. Likewise, the denaturation of the protein as a function of the temperature is also synchronized with the plasma or gamma ray treatment. Nevertheless, the addition of ILs, such as TEMS and TBMS, to the myoglobin protein affects the native stability as the protein varies from IL to IL. TEMS stabilizes the native structure of the myoglobin protein in phosphate buffer, but TBMS slightly denatures the protein structure. However, after irradiation with plasma or gamma rays, both ILs try to protect the structure of the protein against the RONS action. However, TEMS IL protects the protein structure in a better way against both plasma and gamma ray treatments. If we compare the chemical denaturation of the plasma and gamma treatment on the myoglobin structure in the presence of ILs, we observe slightly more denaturation during plasma treatment compared to gamma treatment. While studying the thermal denaturation we detected a larger T_m decrease with gamma ray treatment, as compared to plasma treatment in the presence of TBMS IL. This might be due to the plasma species interacting with TBMS and forming various types of interactions affecting the TBMS, protein, and buffer interactions. On the other hand, the combination of TBMS and gamma rays together decreases T_m more (synchronized effect). Besides, the MD simulations demonstrate that TEMS can better counter the denaturation action of H_2O_2 on the myoglobin structure compared to TBMS, and these findings play an important role in protein folding studies and other areas where we want to counter the deleterious action of plasma and gamma rays.

Acknowledgements

This work was supported by MEXT KAKENHI Grant Number 24108009 and JSPS KAKENHI Grant Number JP16H03895. P. A. is thankful to FY 2015 Japan Society for the Promotion of Science (JSPS) invitation fellowship. P. A. and E. H. C. (SRC) acknowledge the program (Grant #2010-0029421) and Leading Foreign Research Institute Recruitment program (Grant # NRF-2016K1A4A3914113) throughout the Basic Science Research Program of the National Research Foundation (NRF) of Korea

and in part by Kwangwoon University 2017. A. E. C. and M. K. were supported by NRF Grant No. 2016M3A7B4025405 and 2017R1D1A1B03035870.

References

1 B. Burnette and R. R. Weichselbaum, *Semin. Radiat. Oncol.*, 2013, **23**, 273–280.
2 S. M. Bentzen, *Nat. Rev. Cancer*, 2006, **6**, 702–713.
3 E. J. Moding, M. B. Kastan and D. G. Kirsch, *Nat. Rev. Drug Discovery*, 2013, **12**, 526–542.
4 M. Niemantsverdriet, M. J. van Goethem, R. Bron, W. Hogewerf, S. Brandenburg, J. A. Langendijk, P. van Luijk and R. P. Coppes, *Int. J. Radiat. Oncol., Biol., Phys.*, 2012, **83**, 1291–1297.
5 J. P. Moussa, *Russ. J. Plant Physiol.*, 2006, **53**, 193–197.
6 T. von Woedtke, S. Reuter, K. Masur and K.-D. Weltmann, *Phys. Rep.*, 2013, **530**, 291–320.
7 M. Yousfi, N. Merbahi, A. Pathak and O. Eichwald, *Fundam. Clin. Pharmacol.*, 2014, **28**, 123–135.
8 J. H. Park, N. Kumar, D. H. Park, M. Yusupov, E. C. Neyts, C. C. Verlackt, A. Bogaerts, M. H. Kang, H. S. Uhm, E. H. Choi and P. Attri, *Sci. Rep.*, 2015, **5**, 13849.
9 K. Masur, K. Masur, K. Wende, A. Barton, A. Schmidt, U. Lindequist, A. Kramer and K.-D. Weltmann, *Wound Repair Regen.*, 2012, **20**, A102.
10 S. Ikehara, H. Sakakita, K. Ishikawa, Y. Akimoto, T. Yamaguchi, M. Yamagishi, J. Kim, M. Ueda, J. Ikeda, H. Nakanishi, N. Shimizu, M. Hori and Y. Ikehara, *Plasma Processes Polym.*, 2015, **12**, 1348–1353.
11 K. Miyamoto, S. Ikehara, H. Takei, Y. Akimoto, H. Sakakita, K. Ishikawa, M. Ueda, J. Ikeda, M. Yamagishi, J. Kim, T. Yamaguchi, H. Nakanishi, T. Shimizu, N. Shimizu, M. Hori and Y. Ikehara, *Arch. Biochem. Biophys.*, 2016, **605**, 95–101.
12 P. Attri, Y. H. Kim, D. H. Park, J. H. Park, Y. J. Hong, H. S. Uhm, K.-N. Kim, A. Fridman and E. H. Choi, *Sci. Rep.*, 2015, **5**, 9332.
13 P. Attri, M. Yusupov, J. H. Park, L. P. Lingamdinne, J. R. Koduru, M. Shiratani, E. H. Choi and A. Bogaerts, *Sci. Rep.*, 2016, **6**, 34419.
14 P. Bruggeman and C. Leys, *J. Phys. D: Appl. Phys.*, 2009, **42**, 053001.
15 M. Keidar, A. Shashurin, O. Volotskova, M. A. Stepp, P. Srinivasan, A. Sandler and B. Trink, *Phys. Plasmas*, 2013, **20**, 057101.
16 D. Yan, H. Xiao, W. Zhu, N. Nourmohammadi, L. G. Zhang, K. Bian and M. Keidar, *J. Phys. D: Appl. Phys.*, 2017, **50**, 055401.
17 N. Kumar, P. Attri, D. K. Yadav, J. Choi, E. H. Choi and H. S. Uhm, *Sci. Rep.*, 2014, **4**, 7589.
18 N. Kumar, J. H. Park, S. N. Jeon, B. S. Park, E. H. Choi and P. Attri, *J. Phys. D: Appl. Phys.*, 2016, **49**, 115401.
19 A. Ali, Z. Ashraf, N. Kumar, M. Rafiq, F. Jabeen, J. H. Park, K. H. Choi, S. H. Lee, S.-Y. Seo, E. H. Choi and P. Attri, *Sci. Rep.*, 2016, **6**, 21779.
20 M. Vandamme, E. Robert, S. Dozias, J. Sobilo, S. Lerondel, A. L. Pape and J.-M. Pouvesle, *Plasma Medicine*, 2011, **1**, 27–43.
21 L. Brullé, M. Vandamme, D. Riès, E. Martel, E. Robert, S. Lerondel, V. Trichet, S. Richard, J.-M. Pouvesle and A. L. Pape, *PLoS One*, 2012, **7**, e52653.
22 M. Keidar, R. Walk, A. Shashurin, P. Srinivasan, A. Sandler, S. Dasgupta, R. Ravi, R. Guerrero-Preston and B. Trink, *Br. J. Cancer*, 2011, **105**, 1295–1301.
23 M. Vandamme, E. Robert, S. Lerondel, V. Sarron, D. Ries, S. Dozias, J. Sobilo, D. Gosset, C. Kieda, B. Legrain, J.-M. Pouvesle and A. L. Pape, *Int. J. Cancer*, 2012, **130**, 2185–2194.
24 M. Wang, B. Holmes, X. Cheng, W. Zhu, M. Keidar and L. G. Zhang, *PLoS One*, 2013, **8**, e73741.
25 H. J. Lee, C. H. Shon, Y. S. Kim, S. Kim, G. C. Kim and M. G. Kong, *New J. Phys.*, 2009, **11**, 115026.
26 M. Ishaq, M. D. Evans and K. K. Ostrikov, *Biochim. Biophys. Acta, Mol. Cell Res.*, 2014, **1843**, 2827–2837.
27 X. Tan, S. Zhao, Q. Lei, X. Lu, G. He and K. Ostrikov, *PLoS One*, 2014, **9**, e101299.
28 J. Y. Kim, J. Ballato, P. Foy, T. Hawkins, Y. Wei, J. Li and S.-O. Kim, *Biosens. Bioelectron.*, 2011, **28**, 333–338.
29 M. Thiyagarajan, H. Anderson and X. F. Gonzales, *Biotechnol. Bioeng.*, 2014, **111**, 565–574.
30 J. H. Park, M. Kim, M. Shiratani, A. E. Cho, E. H. Choi and P. Attri, *Sci. Rep.*, 2016, **6**, 35883.
31 S. Choi, P. Attri, I. Lee, J. Oh, J.-H. Yun, J. H. Park, E. H. Choi and W. Lee, *Sci. Rep.*, 2017, **7**, 1027.
32 P. Attri, J. Gaur, S. Choi, M. Kim, R. Bhatia, N. Kumar, J. H. Park, A. E. Cho, E. H. Choi and W. Lee, *Sci. Rep.*, 2017, **7**, 2636.
33 P. Attri, N. Kumar, J. H. Park, D. K. Yadav, S. Choi, H. S. Uhm, I. T. Kim, E. H. Choi and W. Lee, *Sci. Rep.*, 2015, **5**, 08221.
34 P. Attri, T. Sarinont, M. Kim, T. Amano, K. Koga, A. E. Cho, E. H. Choi and M. Shiratani, *Sci. Rep.*, 2015, **5**, 17781.
35 H. Zhang, Z. Xu, J. Shen, X. Li, L. Ding, J. Ma, Y. Lan, W. Xia, C. Cheng, Q. Sun, Z. Zhang and P. K. Chu, *Sci. Rep.*, 2015, **5**, 10031.
36 E. Takai, K. Kitano, J. Kuwabara and K. Shiraki, *Plasma Processes Polym.*, 2012, **9**, 77–82.
37 Y. Yu, J. Wang, Q. Shao, J. Shi and W. Zhu, *Sci. Rep.*, 2016, **6**, 19500.
38 P. Attri and P. Venkatesu, *Process Biochem.*, 2013, **48**, 462–470.
39 P. Attri, P. Venkatesu and M.-J. Lee, *J. Phys. Chem. B*, 2010, **114**, 1471–1478.
40 P. Attri and P. Venkatesu, *Phys. Chem. Chem. Phys.*, 2011, **13**, 6566–6575.
41 P. Attri, P. Venkatesu and A. Kumar, *Phys. Chem. Chem. Phys.*, 2011, **13**, 2788–2796.
42 P. Attri, M. Kim, T. Sarinont, E. H. Choi, H. Seo, A. E. Cho, K. Koga and M. Shiratani, *Sci. Rep.*, 2017, accepted.
43 P. Attri, P. Venkatesu, A. Kumar and N. Byrne, *Phys. Chem. Chem. Phys.*, 2011, **13**, 17023–17026.
44 R. Buchfink, A. Tischer, G. Patil, R. Rudolph and C. Lange, *J. Biotechnol.*, 2010, **150**, 64–72.

45 C. Lange, G. Patil and R. Rudolph, *Protein Sci.*, 2005, **14**, 2693–2701.
46 F. van Rantwijk, R. M. Lau and R. A. Sheldon, *Trends Biotechnol.*, 2003, **21**, 131–138.
47 R. A. Sheldon, R. M. Lau, M. J. Sorgedrager, F. van Rantwijk and K. R. Seddon, *Green Chem.*, 2002, **4**, 147–151.
48 P. Attri, P. M. Reddy, P. Venkatesu, A. Kumar and T. Hofman, *J. Phys. Chem. B*, 2010, **114**, 6126–6133.
49 P. Attri, P. Venkatesu and A. Kumar, *J. Phys. Chem. B*, 2010, **114**, 13415–13425.
50 P. Attri, P. Venkatesu and T. Hofman, *J. Phys. Chem. B*, 2011, **115**, 10086–10097.
51 P. Attri, K. Y. Baik, P. Venkatesu, I. T. Kim and E. H. Choi, *PLoS One*, 2014, **9**, e86530.
52 M. Armand, F. Endres, D. R. MacFarlane, H. Ohno and B. Scrosati, *Nat. Mater.*, 2009, **8**, 621–629.
53 K. S. Egorova, E. G. Gordeev and V. P. Ananikov, *Chem. Rev.*, 2017, **117**, 7132–7189.
54 A. Kimura, N. Nagasawa, A. Shimada and M. Taguchi, *Radiat. Phys. Chem.*, 2016, **124**, 130–134.
55 R. P. Morco, A. Y. Musa, M. Momeni and J. C. Wren, *Corros. Sci.*, 2016, **102**, 1–15.
56 P. Attri and E. H. Choi, *PLoS One*, 2013, **8**, e75096.
57 V. D. Noto, M. Piga, G. A. Giffin, S. Lavina, E. S. Smotkin, J.-Y. Sanchez and C. Iojoiu, *J. Phys. Chem. C*, 2012, **116**, 1361–1369.
58 T. Sarinont, T. Amano, P. Attri, K. Koga, N. Hayashi and M. Shiratania, *Arch. Biochem. Biophys.*, 2016, **605**, 129–140.
59 C. M. Jones, *J. Chem. Educ.*, 1997, **74**, 1306.
60 O. C. Fiebig, E. Mancini, G. Caputo and T. D. Vaden, *J. Phys. Chem. B*, 2014, **118**, 406–412.
61 *Impact, version 6.6*, Schrödinger, LLC, New York, NY, 2015.
62 *Desmond Molecular Dynamics System, version 4.4*, D. E. Shaw Research, New York, NY.
63 *Jaguar, version 8.7*, Schrödinger, LLC, New York, NY, 2015.
64 M. C. Miller, S. L. Hanna, K. G. DeFrates, O. C. Fiebig and T. D. Vaden, *Int. J. Biol. Macromol.*, 2016, **85**, 200–207.
65 E. Reichert, R. Wintringer, D. A. Volmer and R. Hempelmann, *Phys. Chem. Chem. Phys.*, 2012, **14**, 5214–5221.
66 J. A. LaVerne, *Radiat. Res.*, 2000, **153**, 196–200.

